Prospectives for bio-oil upgrading via esterification over zeolite catalysts

Originally published in:
Catalysis Today 235, https://doi.org/10.1016/j.cattod.2014.02.047

Funding acknowledgement:
134572 - A fundamental approach to the scale up of hierarchical zeolite catalysts (SNF)

Prospectives for bio-oil upgrading via esterification over zeolite catalysts

*Maria Milina, Sharon Mitchell, and Javier Pérez-Ramírez**

Institute for Chemical and Bioengineering, Department of Chemistry and Applied Biosciences, ETH Zurich, Vladimir-Prelog-Weg 1, CH-8093 Zurich, Switzerland.

* Corresponding author. Tel: +41 44 633 7120; Fax: +41 44 633 1405; E-mail: jpr@chem.ethz.ch

A promising route to upgrade crude bio-oil prior to hydrotreating is via the catalytic esterification of intrinsic acids and alcohols. This process reduces the acidity and oxygen content of bio-oil, thereby improving the stability and decreasing the hydrogen consumption in subsequent refining steps. Here, the applicability of microporous zeolite catalysts for bio-oil esterification is explored in the liquid-phase reaction between the characteristic bio-oil constituents, acetic acid and *o*-cresol. Medium- and large-pore zeolites of different framework type and composition are evaluated, and the highest reactant conversions and product yield are shown to be attained over faujasite and beta zeolites. Ester formation, which is significantly influenced by concurrent coke-forming reactions, is strongly dependent on the reaction temperature and the framework type of the zeolite. The benefits of introducing secondary mesoporosity through demetallation in alkaline media relate to the extent of diffusion constraints and the equilibrium limitation, increasing the conversion of acetic acid by up to a 40% over the optimal faujasite zeolite, in comparison with 200% in the case of ZSM-5. Characterization of the spent catalysts by XRD and N_2 sorption evidences the preserved crystallinity and microporosity of the zeolites, while IR spectroscopy of adsorbed pyridine reveals a small reduction in the concentration of Brønsted acid sites. The latter is detrimental for the ester formation upon reuse of ZSM-5 zeolites, while faujasite catalysts preserve their initial activity. These findings highlight the potential and the possible challenges on application of microporous zeolites and their hierarchical analogues for acid-catalyzed condensation reactions in the field of bio-oil upgrading.

***Keywords*:** Bio-oil Upgrading; Esterification; Zeolite; Hierarchical Zeolite; Demetallation.

1. Introduction

Biomass-derived pyrolysis oils, or bio-oils, are promising candidates to replace petroleum fuels. However, their direct application within existing infrastructure is impeded by their high oxygen content (20-50 wt.%) and acidity (pH = 2.5-3), which impart undesirable properties such as low heating value, immiscibility with hydrocarbon fuels, thermal and chemical instability, high viscosity, and corrosiveness [1,2]. The upgrading of bio-oils to conventional fuels requires the removal of oxygen to within a few wt.%, which can be accomplished by zeolite cracking or hydrotreating [3-5]. While hydrotreating is considered to have the greatest potential to obtain high-grade fuels, its economic viability is limited by the identification of stable catalysts and the hydrogen consumption [6,7]. Currently, a catalytic cascade approach, aimed at exploiting the intrinsic reactivity of the oxygen-containing functional groups (*i.e.* alcohols, acids, aldehydes, ketones) prior to hydrotreating (Fig. 1), is seen as a promising solution to facilitate the upgrading process [8]. In this context, the integration of an esterification step would attractively reduce the acid concentration, thereby improving the stability [9]. Additionally, as with other condensation reactions such as ketonization and aldol condensation, this would enable the partial elimination of oxygen in the form of water, benefiting the process economics by reducing the amount of hydrogen required in succeeding steps.

The removal of carboxylic acids from bio-oils via esterification has been commonly approached through the addition of an external alcohol, such as methanol or ethanol [10]. Together with reducing the pH, the alcohol introduced acts as a solvent, immediately decreasing the viscosity and increasing the heating value [11]. Several recent studies have reported enhancements in the bio-oil quality on tandem application of external alcohols with solid acid catalysts, including resins [9,12-14] and zeolites [15]. However, this would bring little benefit upon further hydrotreating of the bio-oil, as the oxygen content is unaltered. Additionally, this route relies on the availability and price of sustainably produced alcohols.

An alternative, but largely neglected, strategy is the direct catalytic esterification of bio-oil constituents. Comprising a major fraction of alcohols in pyrolysis oil (3-22 wt.%) [16], phenolic compounds are considerably less reactive than methanol or ethanol requiring more severe process conditions [17]. In turn, this introduces increased complexity in the design of a suitable esterification catalyst, especially in relation to their stability in aqueous acidic medium. Under these circumstances, acidic zeolites would represent an adequate choice of the catalysts in view of their high (hydro-)thermal stability, intrinsic acidity, and synthesis flexibility resulting in materials with various pore size, Si/Al ratio, acid site distribution, and hydrophobicity [18]. However, due to relatively large size of the phenolic alcohols with respect to the micropore dimensions in zeolites, significant mass transfer limitations can be expected. Consequently, the use of hierarchical zeolites containing an auxiliary network of mesopores could be highly beneficial. Hierarchical analogues of virtually any family of commercial zeolites can now be prepared through the different strategies available [19, 20], and have demonstrated superior performance in many traditional and emerging applications, including bioenergy related processes such as biomass catalytic pyrolysis [21-23] and bio-oil deoxygenation [24,25].

Here, we assess the potential of zeolite catalysts for bio-oil upgrading via esterification in the liquid-phase reaction between acetic acid and *o*-cresol, characteristic acid and alcohol compounds present in bio-oil (Fig. 1). First, the esterification performance of various microporous zeolites of different framework-type (FER, MFI, MOR, BEA, FAU) and composition (Si/Al = 3-1000) is evaluated at different temperatures. Second, the influence of the introduction of intracrystalline mesopores is evaluated. For this purpose, hierarchical faujasite and ZSM-5 zeolites were prepared by means of alkaline treatment followed by an optional sequential acid wash. The relative impact of the mesopore surface area is assessed in relation to the extent of diffusion constraints. Additionally, we address the important aspect of catalyst reusability and stability in the acidic reaction medium.

2. Experimental

2.1. Catalysts

An overview of the various commercial ferrierite (FER), ZSM-5 (MFI), mordenite (MOR), beta (BEA), and faujasite (FAU) zeolites applied in this work, including the sample codes, manufacturers, chemical composition, and textural properties is provided in Table 1. An amorphous silica-alumina (ASA) was used as non-zeolitic reference materials. The zeolites in NH_4-form were calcined at 823 K for 5 h with a heating ramp of 5 K min^{-1} in static air to attain the H-form. The FAU15 and MFI40 zeolites were alkaline treated in stirred aqueous NaOH solutions (0.1–0.3 M, 338 K, 30 min, 30 cm^3 per gram of zeolite) in the absence (MFI40) or presence (FAU15) of tetrapropylammonium bromide (TPABr, 0.2 M) using an Easymax™ 102 (Mettler Toledo). The suspensions were then quenched in ice-water and filtered, and the isolated solids were washed extensively with distilled water and dried at 338 K. This yielded the alkaline-treated samples denoted AT*x*, where *x* relates to the NaOH concentration applied (*i.e.*, 1 = 0.1 M to 3 = 0.3 M). MFI40-AT*x* samples were subjected to acid washing in aqueous HCl solution (0.1 M, 338 K, 6 h, 100 cm^3 per gram of zeolite) resulting in MFI40-AT*x*-AW catalysts. The alkaline and acid-treated zeolites were converted into the protonic form by three consecutive ion exchange treatments in aqueous NH_4NO_3 (0.1 M, 298 K, 12 h, 100 cm^3 per gram of zeolite), followed by calcination as described above.

2.2 Catalyst characterization

N_2 isotherms at 77 K were measured in a Quantachrome Quadrasorb-SI analyzer following evacuation of the samples at 573 K for 10 h. Powder XRD was conducted by using a PANalytical X'Pert-Pro diffractometer (Bragg-Brentano geometry). Data were recorded in the 3–60º 2θ range with an angular step size of 0.05º and a counting time of 8 s per step. Fourier transform infrared spectroscopy (FTIR) of adsorbed pyridine was conducted in a Bruker IFS 66 spectrometer

(650-4000 cm^{-1}, 2cm^{-1} optical resolution, co-addition of 32 scans). Self-supporting wafers of zeolite (5 ton cm^{-2}, 20 mg, 1 cm^{-2}) were degassed under vacuum (10^{-3} mbar) for 4 h at 693 K, prior to adsorbing pyridine at room temperature. Gaseous and weakly adsorbed molecules were subsequently removed by evacuation at 473 K for 30 min. The total concentrations of Brønsted (c_B) and Lewis (c_L) acid sites were calculated from the band areas of adsorbed pyridine at 1545 cm^{-1} and 1454 cm^{-1}, using the extinction coefficients, ε(B) = 1.67 cm^{-l} mol^{-1} and ε(L) = 2.22 cm^{-l} mol^{-1}, determined previously [26]. The coke content in the spent catalysts was quantified by thermogravimetric analysis in air, conducted using a Mettler Toledo microbalance with a heating ramp of 10 K min^{-1}.

2.3 Catalytic test

The esterification of *o*-cresol with acetic acid was undertaken in glass-pressure tubes (10 cm^3 working volume) between 433 and 493 K under autogenous pressure. The powdered catalyst (50 mg) was added to a mixture containing *o*-cresol (4 mmol, Acros Organics, 99%), acetic acid (2 mmol, Acros Organics, ≥ 99.7%), *n*-octane (1 mmol, Sigma-Aldrich, ≥ 99%), and *p*-xylene (41 mmol, Sigma-Aldrich, ≥ 99%), the latter acted as an internal standard and a solvent, respectively. Following the desired reaction time, the reactors were cooled and the collected liquid samples were analyzed using a gas chromatograph (HP 6890, Hewlett Packard) equipped with a HP-5 capillary column and FID. Reactants and products were calibrated using pure standards. The assignments were confirmed by GC-MS (HP 5973, Hewlett Packard). The conversion of acetic acid (AA) or *o*-cresol (Cr) was calculated as the moles of AA or Cr reacted per mole of AA or Cr fed, whereas the yield of cresol acetate (CrAc) was determined as the moles of CrAc formed per mole of AA fed. Recyclability tests were performed over selected samples under the same conditions described above. Prior to every reuse, the catalysts were calcined in static air at 823 K (2 K min^{-1}) for 5 h. The equilibrium conversion was determined using H_2SO_4 (0.1 mmol, Sigma-Aldrich, 95-87%) as a catalyst.

3. Result and discussion

The results and discussion is divided in four sections; Section 3.1 assesses the activity of various commercial microporous zeolites in the reaction of acetic acid with *o*-cresol; Sections 3.2 and 3.3 investigate the benefit of introducing mesopores by post-synthetic desilication with different severity on the performance of large-pore faujasite and medium-pore ZSM-5 zeolites, respectively; and Section 3.4 elaborates on the catalyst stability and recyclability.

3.1. Esterification over conventional zeolites

Protonated forms of zeolites have been previously investigated as environmentally-benign and reusable alternatives to the mineral acids commonly employed in esterification processes [17,18,27,28]. These studies have identified the pore size (framework type), acid site density, and hydrophobicity of zeolites as critical parameters for an optimal catalyst. Herein, for a first performance comparison, we conducted the reaction of acetic acid with *o*-cresol over various microporous zeolites of different framework type and composition. The porous properties and bulk Si/Al ratios of these catalysts are summarized in Table 1. Fig. 2 illustrates the conversion of acetic acid (X_{AA}) and *o*-cresol (X_{Cr}), and the yield of cresol acetate (Y_{CrAc}) over the zeolites after 1 h of reaction at 453 K. The reaction temperature was chosen to ensure that a reasonable conversion was reached over all zeolites, while negligible autocatalytic contribution (< 5%) was observed in the absence of catalyst under the same conditions. For comparison, the homogeneously catalyzed reaction was also equivalently studied in the presence of 0.1 mmol of H_2SO_4. In general, higher acetic acid conversions of between 30-50% were observed over the large-pore beta and faujasite zeolites than over mordenite, or the medium-pore ZSM-5 or ferrierite zeolites, except in the case of FAU385, which has the lowest aluminum content of all the faujasite catalysts studied. Consistent

with the reactant stoichiometry (AA:Cr = 1:2), a lower relative conversion of *o*-cresol is evidenced. However, in some cases, particularly over zeolites with lower Si/Al ratios (*e.g.* FER10, MFI15, MOR10, and FAU3) the conversion of *o*-cresol was less than half that of the acetic acid. This could originate from the preferential adsorption of the latter reactant in the catalysts, which is particularly noticeable for materials with higher acid site concentrations. Corma *et al*. reported that despite the higher acidity of carboxylic acids with respect to alcohols, the adsorption of protonated acids on the zeolite surface can be favored when an acid-base pair effect is considered [18]. Thus, in addition to the protonation of the carbonyl group by the zeolitic Brønsted sites, an interaction of the hydroxyl group of the organic acid with basic oxygen groups of the zeolite will be important. Besides, acetic acid may be adsorbed preferentially to *o*-cresol in medium-pore zeolites due to its molecular size.

Significantly, no ester or any other product formation was evidenced over the medium-pore zeolites by GC analysis under these conditions, indicating that the reduced concentrations of the reactants observed over these catalysts can be attributed to their adsorption and/or participation in coke forming reactions. Phenolic compounds such as cresols have previously been reported to have a high tendency towards polymerization, especially in the presence of carboxylic acids [29]. Additionally, the formation and subsequent retention of cresol acetate over ferrierite and ZSM-5 zeolites, or further transformation to coking species is possible. In contrast, the large-pore mordenite, beta, and faujasite zeolites demonstrated yields of cresol acetate of up to 25%. Interestingly, whereas virtually identical ester yields were reached over the beta zeolites in a wide compositional window (Si/Al = 13-220), the catalytic activity of faujasite zeolites goes through a maximum at Si/Al = 15 (FAU15). The latter can be explained by a combination of factors; the density and strength of Brønsted acid sites and the zeolite hydrophobicity which vary with the aluminum content of the framework [18].

In order to evaluate the influence of reaction temperature, the esterification was conducted over selected catalysts between 433 and 493 K for 1 h (Fig. 3). The conversion of acetic acid increased

linearly with temperature over both large-pore zeolites, reaching more than 60% at 493 K. Correspondingly, the yield of cresol acetate over these catalysts mirrored the trend in the conversion of acetic acid, except at the highest temperature studied where the reduction in Y_{CrAc} suggests an increased prevalence of coking reactions. In contrast, over the MFI zeolite cresol acetate formation was only appreciably noted at temperatures above 470 K, at which point both X_{AA} and Y_{CrAc} increased in parallel. These findings confirm the superior esterification performance of the large-pore zeolites, but also highlight the narrow window of suitable operating conditions, the range of which is restricted by the high temperature required to induce significant conversions, and the counterproductive rapid coking rates observed under these conditions. For this reason, the yield of cresol acetate would appear a preferential indicator of the catalyst performance since maximization of this parameter will ensure a lower extent of coke formation and/or product inhibition. However, the conversion of acetic acid provides a direct indicator of the efficiency of acid removal, which is one of the primary goals of esterification.

Fig. 4 shows the evolution of reactants and products with reaction time over the large-pore zeolites FAU15 at 453 K, chosen as an optimal catalyst among the faujasite family. The reaction reached equilibrium after approximately 1 h with X_{AA} of *ca*. 50%. However, the equilibrium conversion of acetic acid obtained using sulfuric acid as catalyst was 61% (after 14 h of reaction). The lower equilibrium conversion reached over the zeolite in comparison with the homogenous catalysts could be attributed to the catalyst deactivation, possibly by blockage of the active sites by coke or by strong adsorption of water formed during the esterification reaction. In practice, the equilibrium yield can be increased by the continuous removal of one of the products (ester or water) by distillation; however, this solution would not be very straightforward in the case of real bio-oil processing due to the wide range of boiling points of the complex component mixture.

3.2. Esterification over hierarchical zeolites

It is common knowledge that molecular diffusion to and from active sites within microporous catalysts often limits the performance. To overcome this problem, application of hierarchically structured zeolites, possessing a complementary network of mesopores, have been intensively investigated. The superior performance of hierarchical zeolites, enabled by shortening the diffusion path or by the provision of a larger external surface area available for the reaction, has been demonstrated in many catalytic applications of industrial relevance [29,30]. The introduction of intracrystalline mesopores can be achieved through numerous templating or demetallation strategies. Here, we employed alkaline-mediated desilication treatment as a simple, versatile, and scalable approach. The optimal performing large-pore FAU15 and medium-pore MFI40 zeolites were compared to quantify the impact of different extents of transport limitation on the potential benefits of post-synthetic modification.

3.2.1. Hierarchical FAU zeolites

Following previously established protocol [31], FAU15 was subjected to sodium hydroxide treatment (0.1-0.3 M) in the presence of tetrapropylammonium bromide (0.2 M) as the pore-directing agent. The porous properties of the resulting alkaline-treated zeolites are summarized in Table 2. Mesopore surface area (S_{meso}) and mesopore volume (V_{meso}) increased gradually with increasing NaOH concentration, reaching up to 4 and 3 times higher values than those of the conventional counterpart, respectively. At the same time, a noticeable decrease in micropore volume was only seen for the most severely treated zeolite (FAU15-AT3). The concentrations of Brønsted (c_B) and Lewis (c_L) acid sites in the catalysts were quantified by FTIR study of adsorbed pyridine using the integrated area of the respective bands at 1545 cm^{-1} and 1454 cm^{-1}. The interrelation between the concentration of acid sites and the mesopore surface area developed is shown in Fig. 5a. Whereas a relatively minor

reduction in c_B was observed for the zeolites with S_{meso} < 300 m^2 g^{-1}, a more pronounced loss (36%) was evidenced for the most mesoporous FAU15-AT3, coinciding with the drop in V_{micro}. A close to linear trend was observed between c_L and S_{meso} in agreement with the previously reported relationship for MFI zeolites [32,33].

The conversion of acetic acid and the yield of cresol acetate at 453 K after 30 min of reaction *versus* the mesopore surface area of the zeolites are depicted in Fig. 5b. While both X_{AA} and Y_{CrAc} initially rise gradually with the developed S_{meso}, as larger mesopore surface areas are introduced, the enhancing effect tends towards a maximum conversion of X_{AA} = 56% and Y_{CrAc} = 28%. This could be attributed to the more significant drop in the amount of Brønsted acid sites verified for this catalyst. However, this conversion and yield are also approaching the equilibrium values identified in Fig. 4, which could limit the potential benefits of mesoporosity introduction in active large-pore zeolites

3.2.2. Hierarchical MFI zeolites

Despite the lower activity of MFI in comparison with FAU zeolites, its potential application in bio-oil esterification was investigated in view of the higher stability reported in the presence of hot liquid water [35]. In recent work, we have described in detail the range of achievable porous properties in MFI40 zeolites upon variation of the base concentration during alkaline treatment and characterized the interdependence between the porous and acidic properties [32]. It has been also demonstrated that for reactions with strong acidity requirements, catalysts treated at NaOH concentration above 0.3 M provide only little or no catalytic benefits due to the reduced concentration and strength of Brønsted acid sites. Therefore, in this study the zeolites prepared at NaOH concentration ≤ 0.3 M were tested. Additionally, the desilicated zeolites were sequentially acid-washed with a mild HCl solution (0.1 M) to remove aluminum species redistributed during alkaline treatment. The porous and acidic properties of these zeolites are reported in [32].

The evolution of the concentration of acetic acid and cresol acetate over the conventional MFI40 and the most mesoporous alkaline-treated (MFI40-AT3) and acid-washed (MFI40-AT3-AW) zeolites is shown in Fig. 6a. The benefits of mesoporosity introduction are clearly seen in the improved X_{AA} and Y_{CrAc} reaching up to 3 and 4.5 times higher values than those of the conventional zeolites. The conversion of acetic acid and *o*-cresol (not shown for clarity) increased continually during the entire catalytic run, whereas the yield of cresol acetate stayed constant or decreased after 4 h of reaction, suggesting that the ester product polymerizes at longer reaction times. For this reason, the performance of the catalysts was compared after 4 h of reaction. The relation between the conversion of acetic acid over the conventional and modified zeolites and the mesopore surface area is demonstrated in Fig. 6b. Although not shown for brevity, equivalent trends were also observed in the ester yield. The linear increase is expected due to the access-limited nature of this esterification in the MFI zeolite crystals (*i.e.* the kinetic diameter of cresol acetate is greater that the micropore diameter). Acid-washed samples followed the same trend, exhibiting slightly elevated acetic acid conversions and ester yields, which could be attributed to the higher accessibility of the acid sites due to removal of aluminum-containing species residual from the alkaline treatment [32]. An inferior activity was observed over the amorphous silica alumina (ASA) reference due to its lower concentration and strength of Brønsted acid sites. Nevertheless, an appreciable amount of cresol acetate formed over the ASA catalyst. The higher relative improvement observed upon mesoporosity introduction in MFI40 in contrast to FAU15 zeolite correlates well with the degree of mass transport limitations within the conventional catalysts and consequently the lower initial activity of the MFI40 zeolite.

3.3. Catalyst stability and recyclability

Catalyst stability can be envisaged as a significant challenge for the potential use of zeolite catalysts in bio-oil upgrading. To assess the impact of the reaction conditions on the catalyst properties, the

selected zeolites were characterized after use following oxidative regeneration and their performance was evaluated in consecutive runs. Due to the challenges associated with quantifying the amount of coke deposited in zeolites applied in liquid-phase batch systems, a detailed comparison is not presented. In general, both soft and hard (*ca.* 6-10wt.%) coke species were observed over all catalysts, with slightly increased amounts of hard coke evidenced over the hierarchical zeolites in agreement with the higher activity. As summarized in Fig. 7, the conversion of acetic acid over all zeolites remained constant or slightly increased in the second and/or third cycle, which could be attributed to the higher external surface area evidenced by N_2 sorption in the catalysts after the first catalytic run (for FAU15 and FAU15-AT2 shown in Table 2 and Fig. 8a). Notably, the original micropore volume was virtually unaffected, highlighting the stability of the zeolite frameworks under the conditions studied. This was further confirmed by the fully preserved crystallinity verified by X-ray diffraction (Fig. 8b). IR spectroscopy of adsorbed pyridine demonstrated a slight decrease in the concentration of Brønsted acid sites, whereas the concentration of Lewis acid sites remained constant (Fig. 8c). The expected progressive decrease in c_B with each catalytic cycle could be responsible for the reduced yield of cresol acetate in consecutive runs, which was especially pronounced for the conventional and hierarchical MFI40 zeolites. In contrast to MFI40, the FAU15 zeolite demonstrated an enhanced Y_{CrAc} in the second cycle, which was retained in the third. Although, the cause of this is not yet clear, it could possibly originate either from increased accessibility of the acid sites upon removal of extra-framework Al-species in the acidic esterification environment or from the selective dealumination of the framework leading to the increased strength of remaining acid sites. This would require further investigation. In summary, these finding show that zeolite catalysts would suffer from dealumination phenomena in the highly acidic bio-oil media, therefore substantial efforts should be made on studying stability of zeolites or any other catalysts

when considering bio-oil upgrading application via condensation reactions, whether it is esterification, ketonization, or aldol condensation.

4. Conclusions

This work has provided valuable insights for the preparation and application of zeolite catalysts to improve the properties of bio-oil via esterification, highlighting practical considerations which will determine their success. We have evaluated the performance of the widely used commercial zeolites in the esterification of acetic acid with *o*-cresol, two common bio-oil constituents. A comparative assessment revealed that significant ester formation occurred over large-pore zeolites at 453 K. Appreciable esterification over medium-pore zeolites was only observed at 473 K, whereas reduction in the reactant concentrations at lower temperatures was primarily linked with the strong adsorption within the zeolite and coke forming reactions. The impact of the bulk Si/Al ratio depended on the framework type, reaching a maximum ester yield at intermediate Si/Al ratios for the faujasite catalysts, while equivalent yields were seen over a wide range of compositions for beta zeolites. The reaction conditions were restricted by the high temperature required to catalyze the esterification of phenolic alcohols, which also promoted coke formation. Enhancements in the esterification efficiency upon mesopore development by desilication depended on the relative impact on the acid site concentration and external surface area, the degree of mass transfer limitation, and the relative equilibrium yield, with larger benefits observed over access-limited ZSM-5 than faujasite zeolites. Although the crystallinity and micropore volume were preserved in the acidic hydrothermal conditions of the reaction, the Brønsted acid site density was decreased resulting in the reduced ester yield in consecutive runs, which was especially pronounced over ZSM-5 zeolites. Further studies exploring the stability of zeolite catalysts in greater detail, comparing different catalyst systems and

catalytic routes, and working with real bio-oils are essential milestones to determine the potential of condensation reactions for bio-oil upgrading.

Acknowledgements. The Swiss National Science Foundation (project number 200021-134572) is acknowledged for financial support. Tobias Keller and Gabriele Colombo are thanked for help with catalyst preparation and testing, respectively.

References

[1] A. Oasmaa, S. Czernik, Energy Fuels 13 (1999) 914.

[2] S. Czernik, A. V. Bridgwater, Energy Fuels 18 (2004) 590.

[3] G. Huber, A. Corma, Angew. Chem. Int. Ed. 46 (2007) 7184.

[4] P. M. Mortensen, J.-D. Grunwaldt, P. A. Jensen, K. G. Knudsen, A. D. Jensen, Appl. Catal. A 407 (2011) 1.

[5] A. V. Bridgwater, Biomass Bioenerg. 38 (2012) 68.

[6] M. M. Wright, D. E. Daugaard, J. A. Satrio, R. C. Brown, Fuel 89 (2010) S2.

[7] D. M. Alonso, J. Q. Bond, J. A. Dumesic, Green Chem. 12 (2010) 1493.

[8] D. E. Resasco, J. Phys. Chem. Lett. 2 (2011) 2294.

[9] J.-J. Wang, J. Chang, J. Fan, Energy Fuels 24 (2010) 3251.

[10] S. Xiu, A. Shahbazi, Renewable Sustainable Energy Rev. 16 (2012) 4406.

[11] J. P. Diebold, S. Czernik, Energy Fuels 11 (1997) 1081.

[12] F. H. Mahfud, I. Melián-Cabrera, R. Manurung, H. J. Heeres, Process Saf. Environ. Prot. 85 (2007) 466.

[13] X. Li, R. Gunawan, C. Lievens, Y. Wang, D. Mourant, S. Wang, H. Wu, M. Garcia-Perez, C.-Z. Li, Fuel 90 (2011) 2530.

[14] X. Hu, R. Gunawan, D. Mourant, C. Lievens, X. Li, S. Zhang, W. Chaiwat, C.-Z. Li, Fuel 97 (2012) 512.

[15] J. Peng, P. Chen, H. Lou, X. Zheng, Bioresour. Technol. 100 (2009) 3415.

[16] A. Mullen, A. A. Boateng, Enerfy Fuels 22 (2008) 2104.

[17] H. E. Hoydonckx, D. E. De Vos, S. A. Chavan, P. A. Jacobs, Top Catal. 27 (2004) 83.

[18] A. Corma, H. Garcia, S. Ibarra, J. Prieto, J. Catal. 120 (1989) 78.

[19] J. Pérez-Ramírez, C. H. Christensen, K. Egeblad, C. H. Christensen, J. C. Groen, Chem. Soc. Rev. 37 (2008) 2530.

[20] D. P. Serrano, J. M. Escola, P. Pizarro, Chem. Soc. Rev. 42 (2013) 4004.

[21] A. J. Foster, J. Jae, Y.-T. Cheng, G. W. Huber, R. F. Lobo, Appl. Catal. A 423-424 (2012) 154.

[22] S. Stefanidis, K. Kalogiannis, E. F. Iliopoulou, A. A. Lappas, J. Martínez Triguero, M. T. Navarro, A. Chica, F. Rey, Green Chem. 15 (2013) 1647.

[23] G. T. Neumann, J. C. Hicks, Top Catal. 55 (2012) 196.

[24] Y. Wang, Y. Fang, T. He, H. Hu, J. Wu, Catal. Commun. 12 (2011) 1201.

[25] H. J. Park, K.-H. Park, J.-K. Jeon, J. Kim, R. Ryoo, K.-E. Jeong, S. H. Park, Y.-K. Park, Fuel 97 (2012) 379.

[26] C. A. Emeis, J. Catal. 141 (1993) 347.

[27] S. R. Kirumakki, N. Nagaraju, K. V. R. Chary, Appl. Catal. A 299 (2006) 185.

[28] J. Bedard, H. Chiang, A. Bhan, J. Catal. 290 (2012) 210.

[29] X. Hu, Y. Wang, D. Mourant, R. Gunawan, C. Lievens, W. Chaiwat, M. Gholizadeh, L. Wu, X. Li, C.-Z. Li, AIChE J. 59 (2013) 888.

[30] M. S. Holm, E. Taarning, K. Egeblad, C. H. Christensen, Catal. Today 168 (2011) 3.

[31] D. Verboekend, G. Vilé, J. Pérez-Ramírez, Adv. Funct. Mater. 22 (2012) 916.

[32] M. Milina, S. Mitchell, N.-L. Michels, J. Kenvin, J. Pérez Ramírez, J. Catal. 308 (2013) 398.

[33] P. Y. Dapsens, C. Mondelli, J. Pérez-Ramírez, ChemSusChem 6 (2013) 831.

[34] D. Verboekend, S. Mitchell, M. Milina, J. C. Groen, J. Pérez-Ramírez, J. Phys. Chem. C 115 (2011) 14193.

[35] R. M. Ravenelle, F. Schüssler, A. D'Amico, N. Danilina, J. A. van Bokhoven, J. A. Lercher, C. W. Jones, C. Sievers, J. Phys. Chem. C 114 (2010) 19582.

Figure captions

Fig. 1. Cascade approach for the production of fuels from biomass, including an intermediate deoxygenation step via condensation reactions. The esterification of *o*-cresol with acetic acid, two characteristic constituents of crude bio-oil, has been investigated in this manuscript.

Fig. 2. Evaluation of zeolite catalysts in the esterification of *o*-cresol (Cr) with acetic acid (AA) resulting in cresol acetate (CrAc). The micropore size increases from left (FER) to right (FAU). The relative performance of sulfuric acid (0.1 mmol) is included for comparison. Conditions: T = 453 K, Cr/AA = 2, W_{cat} = 50 mg, and t = 1 h.

Fig. 3. Conversion of acetic acid (X_{AA}) (a) and yield of cresol acetate (Y_{CrAc}) (b) *versus* reaction temperature in the esterification of *o*-cresol with acetic acid over selected catalysts. Conditions: Cr/AA = 2, W_{cat} = 50 mg, and t = 1 h.

Fig. 4. Concentration profiles of the reactants and product during the esterification of *o*-cresol with acetic acid over FAU15 zeolite. Conditions: T = 453 K, Cr/AA = 2, and W_{cat} = 50 mg.

Fig. 5. Interdependence between the concentration of Brønsted (c_B) and Lewis (c_L) acid sites and the mesopore surface area (S_{meso}) developed in FAU15 zeolite upon alkaline treatment (a). Relationship between the conversion of acetic acid (X_{AA}) and the yield of cresol acetate (Y_{CrAc}) with S_{meso} in the esterification of acetic acid with *o*-cresol. Conditions: T = 453 K, Cr/AA = 2, W_{cat} = 50 mg, and t = 0.5 h.

Fig. 6. Concentration profiles of acetic acid (circles) and cresol acetate (triangles) during the esterification of *o*-cresol over the conventional and modified MFI40 zeolites (a). Relation between the developed mesopore surface area (S_{meso}) and the conversion of acetic acid (X_{AA}) after 4 h of reaction (b). The relative conversion over amorphous silica alumina (ASA) is shown for comparison. Conditions: T = 473 K, Cr/AA = 2, and W_{cat} = 50 mg.

Fig. 7. Conversion of acetic acid (X_{AA}) and yield of cresol acetate (Y_{CrAc}) over selected zeolite catalysts upon reuse in three consecutive runs. Conditions: (a) T = 453 K, Cr/AA = 2, W_{cat} = 50 mg, and t = 0.5 h. (b) T = 473 K, Cr/AA = 2, W_{cat} = 50 mg, and t = 4 h.

Fig. 8. Characterization of FAU15 and FAU15-AT2 catalysts before and after 30 min of reaction at 453 K. N_2 sorption isotherms before (solid symbols) and after (open symbols) esterification (a). X-ray diffraction patterns (b) and FTIR spectra following pyridine adsorption (c) before (grey lines) and after (red and blue lines) esterification.

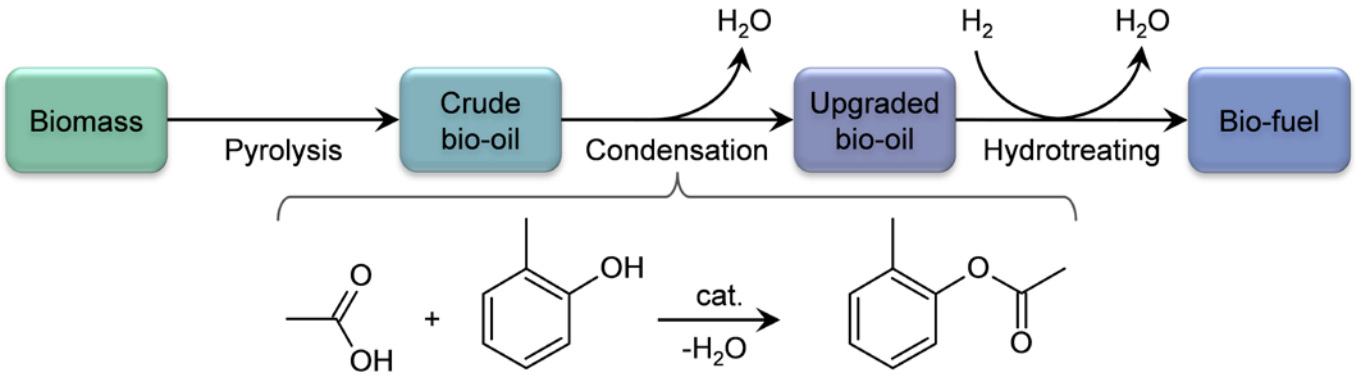
Biomass
Pyrolysis
Crude bio-oil
H_2O
Condensation
Upgraded bio-oil
H_2
H_2O
Hydrotreating
Bio-fuel
O
OH
+
OH
cat.
$-H_2O$
O
O

Fig. 1

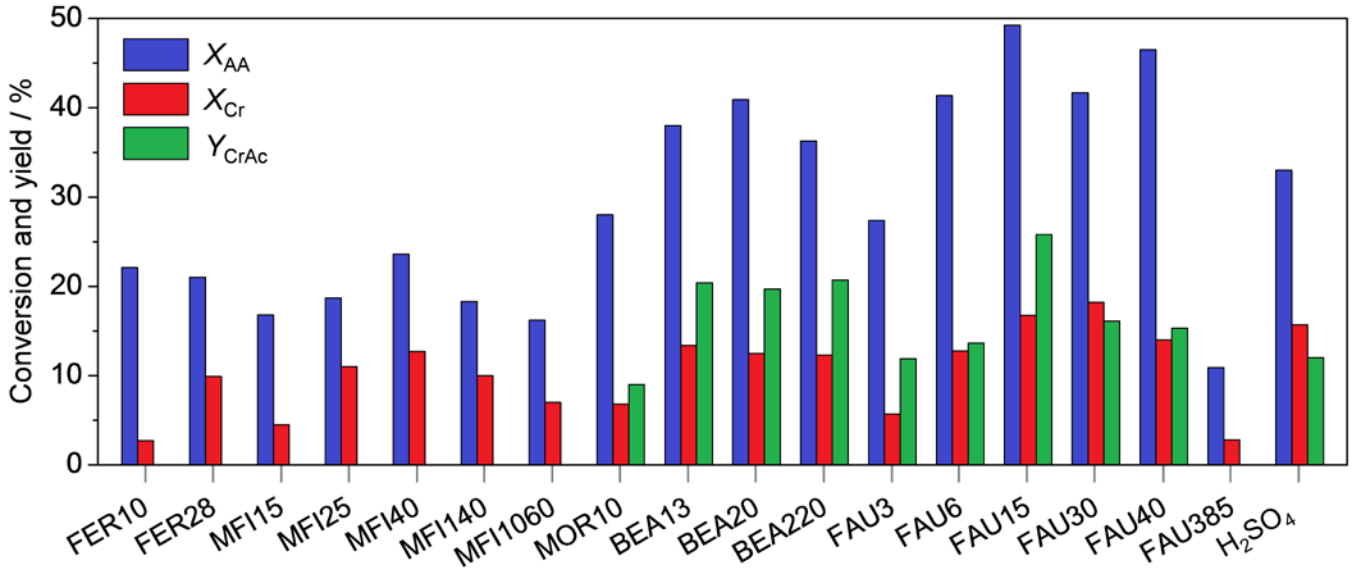
Conversion and yield / %
50
40
30
20
10
0
X_{AA}
X_{Cr}
Y_{CrAc}
FER10
FER28
MFI15
MFI25
MFI40
MFI140
MFI1060
MOR10
BEA13
BEA20
BEA220
FAU3
FAU6
FAU15
FAU30
FAU40
FAU385
H_2SO_4

Figure 2

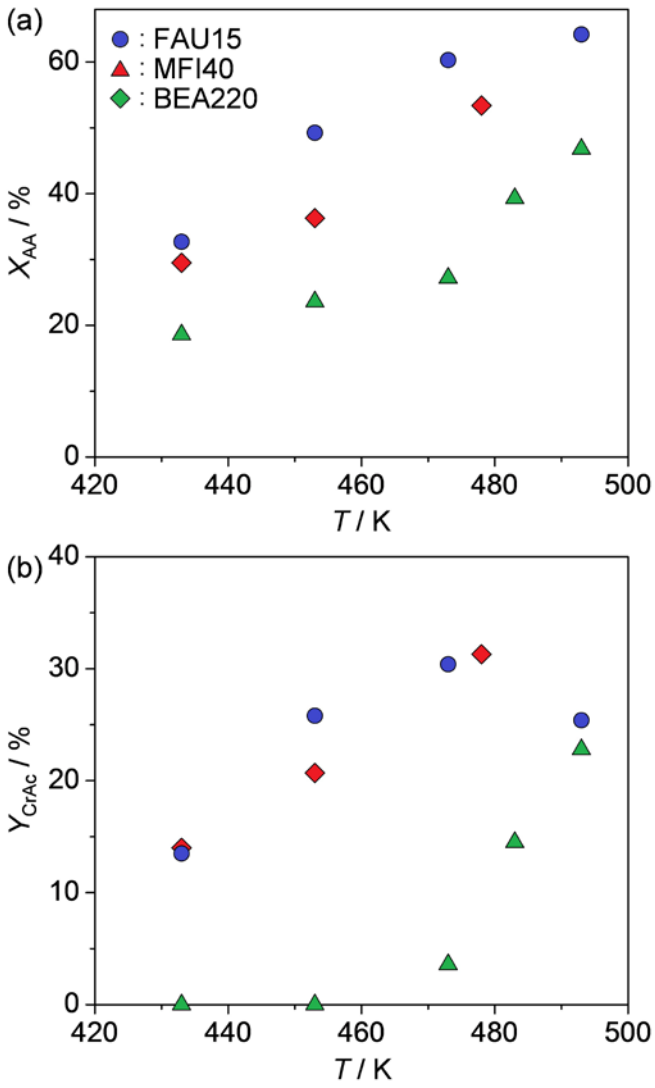
(a)
: FAU15
: MFI40
: BEA220
X_{AA} / %
0
20
40
60
420
440
460
480
500
T / K
(b)
Y_{CrAc} / %
0
10
20
30
40
420
440
460
480
500
T / K

Figure 3

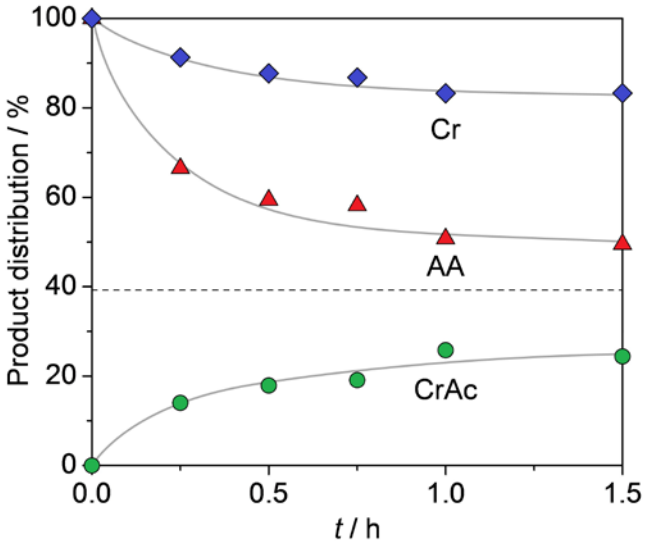

Figure 4

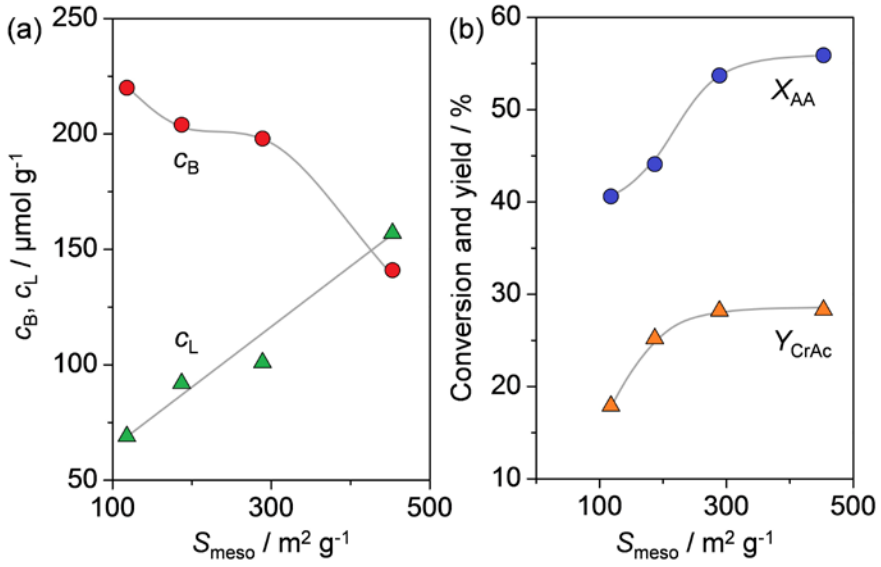
(a)
250
200
150
100
50
100
300
500
c_B, c_L / µmol g^{-1}
c_B
c_L
S_{meso} / m^2 g^{-1}
(b)
60
50
40
30
20
10
100
300
500
Conversion and yield / %
X_{AA}
Y_{CrAc}
S_{meso} / m^2 g^{-1}

Figure 5

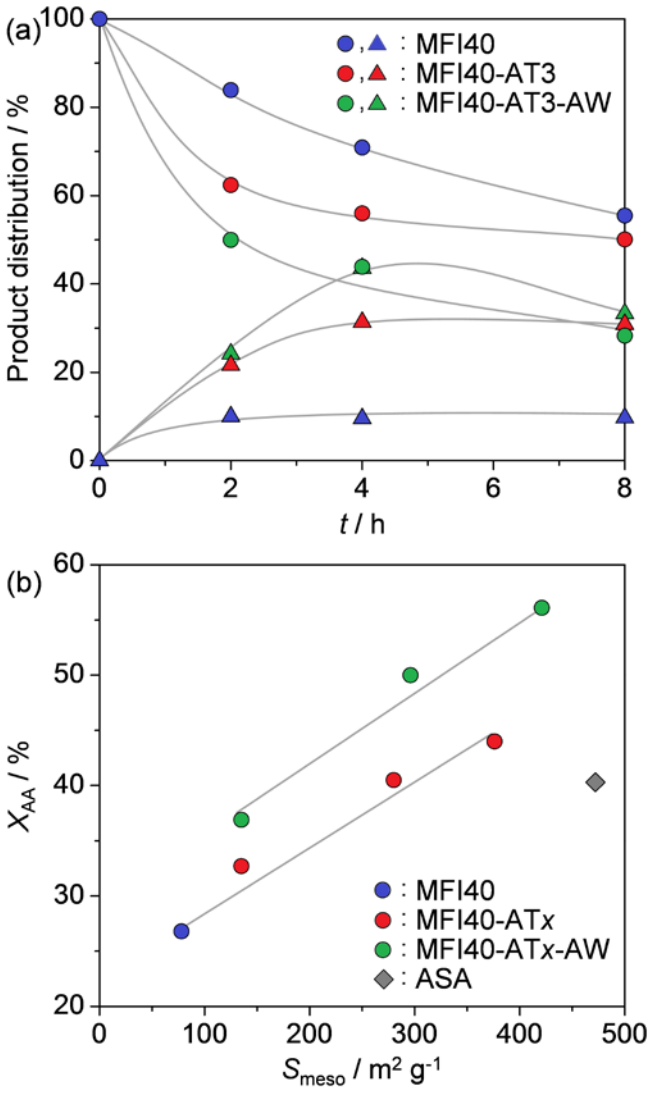
(a)
Product distribution / %
t / h
●,▲ : MFI40
●,▲ : MFI40-AT3
●,▲ : MFI40-AT3-AW
(b)
X_AA / %
S_meso / m² g⁻¹
● : MFI40
● : MFI40-ATx
● : MFI40-ATx-AW
◆ : ASA

Figure 6

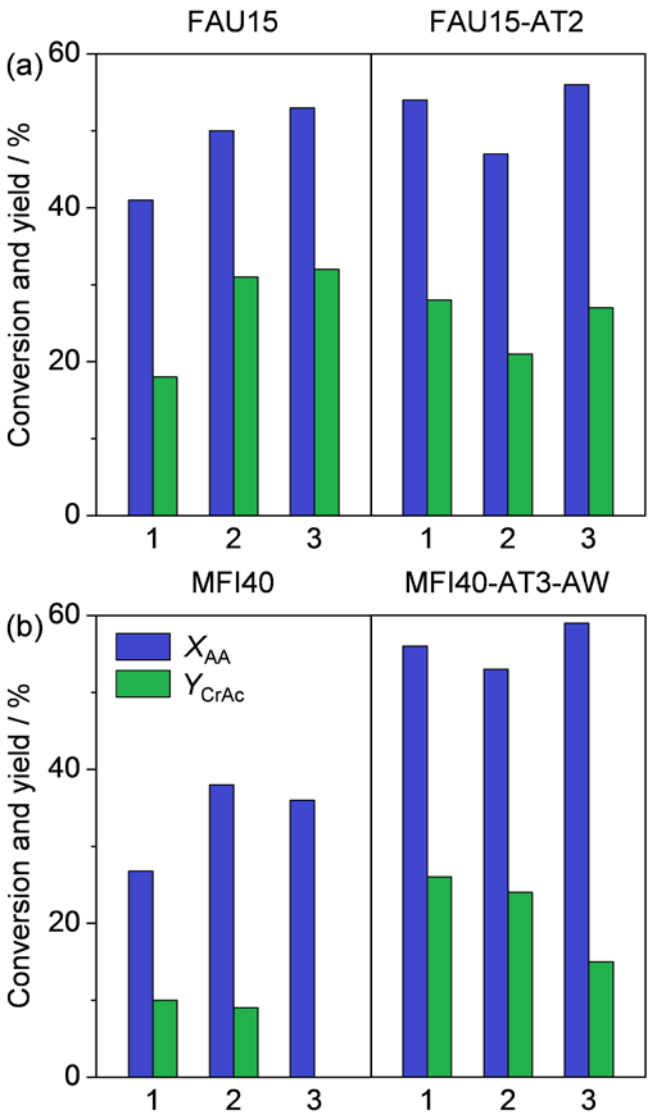
FAU15
FAU15-AT2
(a)
Conversion and yield / %
60
40
20
0
1
2
3
1
2
3
MFI40
MFI40-AT3-AW
(b)
X_{AA}
Y_{CrAc}
Conversion and yield / %
60
40
20
0
1
2
3
1
2
3

Figure 7

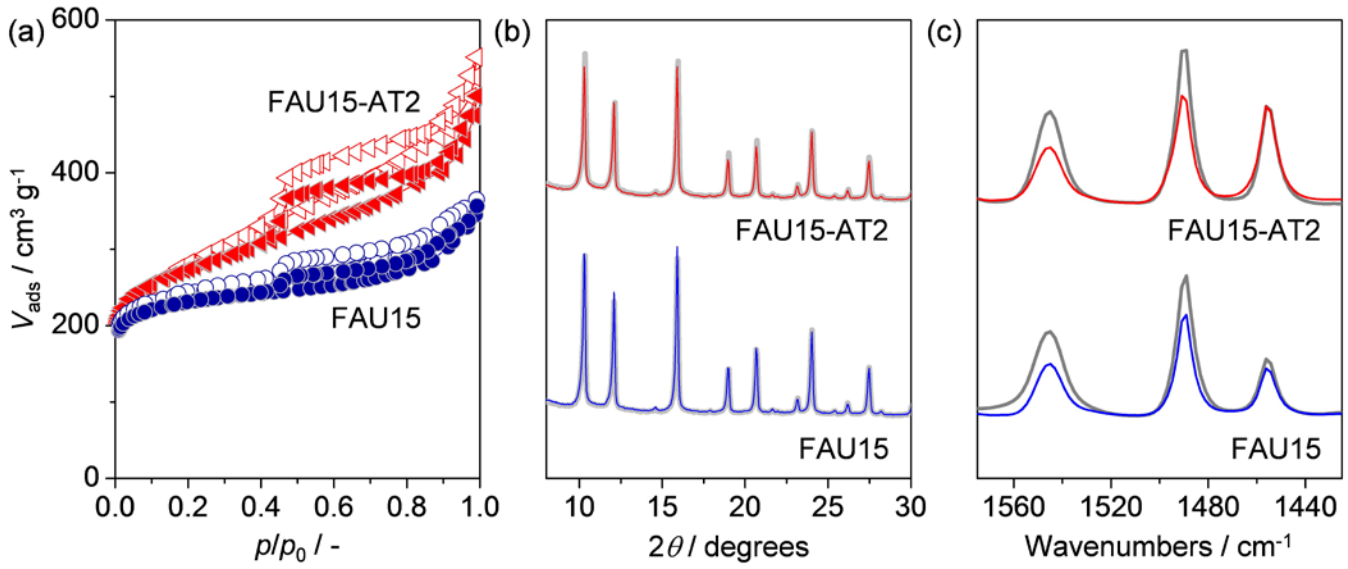
(a)
600
400
200
0
FAU15-AT2
FAU15
V_{ads} / cm^3 g^{-1}
0.0
0.2
0.4
0.6
0.8
1.0
p/p_0 / -
(b)
FAU15-AT2
FAU15
10
15
20
25
30
2θ / degrees
(c)
FAU15-AT2
FAU15
1560
1520
1480
1440
Wavenumbers / cm^{-1}

Figure 8

Table 1. Overview of studied conventional zeolites and their porous properties.

Sample	Provider, code	bulk Si/Al[a] (mol mol^{-1})	S_{BET}[b] (m^2 g^{-1})	S_{meso}[c] (m^2 g^{-1})	V_{micro}[c] (cm^3 g^{-1})	V_{total} (cm^3 g^{-1})
FER10	Zeolyst, CP914C	10	293	24	0.14	0.19
FER28	Zeolyst, CP914	28	347	35	0.13	0.25
MFI15	Zeolyst, CBV3024E	15	412	76	0.14	0.29
MFI26	Zeolyst, CBV5524G	26	461	76	0.17	0.31
MFI40	Zeolyst, CBV8014	40	468	78	0.17	0.28
MFI140	Zeolyst, CBV28014	140	375	135	0.12	0.21
MFI1060	Tosoh, HSZ-890HOA	1060	422	36	0.16	0.18
MOR10	Zeolyst, CBV21A	10	526	42	0.20	0.33
FAU3	Zeolyst, CBV300	2.5	824	20	0.32	0.36
FAU6	Zeolyst, CBV712	6	778	98	0.28	0.45
FAU15	Zeolyst, CBV720	15	872	114	0.31	0.53
FAU30	Zeolyst, CBV760	30	904	113	0.32	0.54
FAU40	Zeolyst, CBV780	40	859	139	0.30	0.54
FAU385	Tosoh, HSZ-390HUA	385	848	100	0.30	0.58
BEA13	Zeolyst, CP814E	12.5	657	221	0.18	0.77
BEA20	Tosoh, HSZ-940HOA	20	600	55	0.23	0.29
BEA220	Tosoh, HSZ-980HOA	220	559	82	0.20	0.34
ASA	Aldrich	13	472	472	0	0.70

[a] according to the manufacturer's specifications. [b] BET method applied to the N_2 isotherm. [c] *t*-plot method.

Table 2. Porous properties of the conventional and alkaline-treated FAU15 zeolites.

Sample[a]	c_{NaOH} (M)	S_{BET}[a] ($m^2\ g^{-1}$)	S_{meso}[b] ($m^2\ g^{-1}$)	V_{micro}[b] ($cm^3\ g^{-1}$)	V_{total} ($cm^3\ g^{-1}$)
FAU15	-	872 (876)[c]	114 (122)	0.31 (0.32)	0.53 (0.54)
FAU15-AT1	0.1	938	187	0.31	0.63
FAU15-AT2	0.2	1013 (1006)	289 (331)	0.30 (0.28)	0.73 (0.81)
FAU15-AT3	0.3	998	453	0.23	0.95

[a] BET method applied to the N_2 isotherm. [b] *t*-plot method. [c] values in parenthesis represent the properties of the catalysts after 30 min of reaction at 453 K followed by calcination.

Highlights

Prospectives for bio-oil upgrading via esterification over zeolite catalysts

*Maria Milina, Sharon Mitchell, and Javier Pérez-Ramírez**

- ► Zeolites shown to be potential catalysts for the esterification of bio-oil constituents.
- ► Efficiency of carboxylic acid removal enhanced by the presence of intracrystalline mesopores.
- ► Benefits upon application of hierarchical zeolites related to extent of transport limitations.
- ► Property alteration due to the acidic hydrothermal conditions identified as challenge for viability.

Graphical abstract